Process chain for serial manufacture of polymer components with micro- and nano-scale features: Optimisation Issues

Vella , Pierre ; Dimov, Stefan; Kolew, Alexander

DOI:
10.1177/0954405415619344

Document Version
Peer reviewed version

Citation for published version (Harvard):
Vella , P, Dimov, S & Kolew, A 2016, 'Process chain for serial manufacture of polymer components with micro- and nano-scale features: Optimisation Issues', *Proceedings of the Institution of Mechanical Engineering Part B Journal of Engineering Manufacture*. https://doi.org/10.1177/0954405415619344

Process chain for serial manufacture of polymer components with micro- and nano-scale features: Optimisation issues

Pierre C Vella[a, b1], Stefan S Dimov[a], Alexander Kolew[c]

[a] *School of Mechanical Engineering, University of Birmingham, Edgbaston, Birmingham, UK*

[b] *Department of Industrial and Manufacturing Engineering, University of Malta, Msida, Malta*

[c] *Karlsruhe Institute of Technology, Karlsruhe, Germany*

Abstract

This paper reports a follow-up research to investigate further the component technologies of a cost effective manufacturing route designed to achieve function and length scale integration (FLSI) in products. The route employs a viable master-making process chain that integrates compatible and at the same time complementary, structuring and replication technologies to fabricate Zr-based bulk metallic glass inserts. To validate them they are subsequently integrated in a micro-injection moulding (µIM) machine and polymer structures incorporating both micro- and nano -scale features are replicated. Especially, the masters and/or replicas after each processing step were analysed and the factors affecting its overall performance were identified. The research demonstrated that the master-making process chain can be a viable fabrication route for both fully amorphous and partially crystalline Zr-based BMG inserts that incorporate different length scale features. The results also showed that relatively good fidelity of the different scale features can be achieved with the µIM process and thus it can enable FLSI in thermoplastic components.

[1] **Corresponding author**.

Email address: pvella@eng.um.edu.mt. **Telephone:** (+356) 2340 2059. **Fax:** (+356) 21343577

Keywords

Micro Manufacturing, Process Chains, Micromilling, Hot Embossing, Focused Ion Beam Milling, Micro-Injection Moulding, Bulk Metallic Glasses, Function and Length Scale Integration, Wear, Fatigue

1.0 Introduction

The global market for miniaturised products has been increasing continuously in the last decade [1] . This is a direct consequence of the growing needs and demands across a range of industry sectors to integrate more functions in the smallest possible packages/components by exploiting the latest advances in functional materials and also by integrating different length scale functional features/structures from meso down to nano scales. This generic trend in miniaturising devices can be concisely defined as an integration of functional multi-scale structures or features into a single component or in short Function and Length Scale Integration (FLSI)[2] .

This FLSI trend has to be underpinned by innovative, reliable and cost effective manufacturing methods for producing components with multi-scale features in a variety of materials. In practice, devices having a complex geometry, which incorporate different scales' features, are difficult and even impossible to produce cost effectively by employing a single process, and therefore necessitate the integration of several compatible and at the same time complementary manufacturing technologies into process chains. Thus, the most important requirement for achieving a high-throughput production of micro- and nano-scale components is the design of viable process chains for their cost-effective fabrication.

Within this context, a cost effective master making process chain for achieving FLSI in mould inserts was designed by the authors (See Figure 1). It employed Zr-based BMG workpieces to integrate compatible and complementary structuring and replication technologies. In particular, first a positive Al-alloy master was manufactured by µMilling and then used to

produce a negative Zr-based BMG insert for micro injection moulding using the Thermo Plastic Forming (TPF) process. After the TPF step, the aluminium master was dissolved to release the structured BMG insert. The third step employed FIB milling to add sub-micron structures on top of the pre-existing BMG insert's micro features. Thus, the BMG insert was structured in two stages, first by TPF to fabricate the meso and micro size features that define the part overall geometry and subsequently by FIB milling to generate a relatively small number of high resolution sub-micron and nano patterns. To validate this FLSI enabling master-making process chain the micro- and nano- structured BMG insert was integrated into an injection moulding tool to produce small batches of thermoplastic devices. These results provided sufficient evidences about the viability of this master making process chain as a fabrication route for serial production of polymer based FLSI devices. However, this was just a feasibility study and all component technologies in the proposed process chain have to undergo further optimisation in the context of any specific application, and also their capabilities have to be studied systematically and potentially developed further.

This paper reports a follow-up research work to investigate the component technologies of this FLSI enabling master-making process chain. In particular, supplementary trials to investigate potential improvements to the surface integrity of the Al masters generated by the µMilling process are presented. Also, an experimental study of the TPF process is carried out to investigate its constraints in regards to the achievable replication quality. The FIB machining response of a fully amorphous Zr-based BMG insert is also systematically studied and subsequently compared with the previously reported results for partially crystalline Zr-based BMG inserts and thus to determine whether there are any differences in the achievable nanoscale feature resolution and surface integrity. Finally, µIM trials are carried out to understand the broader applicability of the proposed FLSI enabling master-making process chain. The effects of BMG partial crystallisation on the insert's wear and fatigue life response is also studied in the context of the proposed process chain.

The rest of the paper is organized as follows. Next section outlines the experimental set-up utilised to carry out the above mentioned investigations. Then, the obtained results and future research directions are discussed, and conclusions are made.

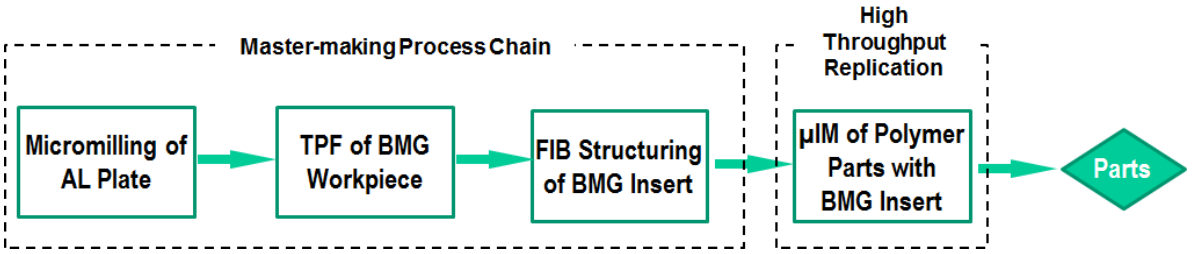

Figure 1. Overall process chain design

2.0 Experimental Setup

2.1 Insert material

The particular BMG used in this study is the commercially available Vitreloy 1b (Vit1b). The mechanical properties of this amorphous alloy are extremely high; in particular its tensile yield strength is 1.9 GPa while its hardness is 540 Hv. Therefore, it is suitable to produce high wear resistant mould inserts for micro injection moulding. In addition, from a master-fabrication viewpoint, Vit 1b has excellent thermoplastic formability[3] . Therefore, it can be fittingly processed by TPF while FIB nano structuring can be used to integrate micro and nano-structures in a master with a high level of surface integrity. In addition, the Vit 1b alloy is resistant to most acids and bases and thus it is also suitable for post processing, namely the selective dissolution of aluminium masters after the TPF process[4] .

2.2 Test structure design

A schematic view of the simple micro-mixer used in this study is shown in Figure 2. Its channel and reservoir features are of micro scale while it also integrates three gratings that are of sub-micron and nano scales. As it is depicted in Figure 3, each grating consists of a pattern of 20 x 20 black or white fields and all white fields are pockets. The smallest pixel dimensions in X, Y and Z directions of Gratings 1, 2 and 3 are 1µm, 600nm and 200nm respectively.

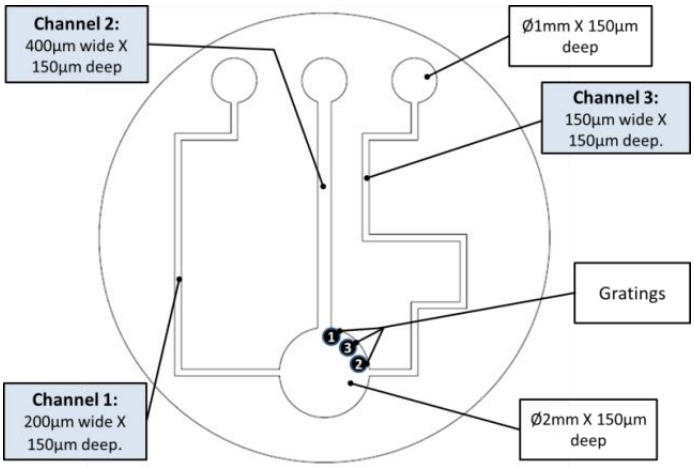

Figure 2. The micro-mixer design

Structure No	X (µm)	Y (µm)
1	20	20
2	12	12
3	4	4

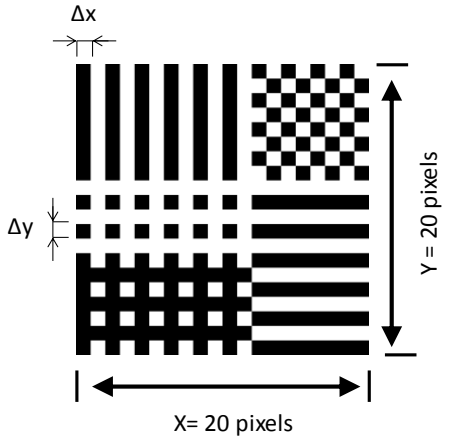

Figure 3. Grating structures

2.3 Micromilling of aluminium master

The µMilling technology was employed to machine the micro-mixer features onto the Al workpieces. A tooling grade Al was used, in particular AL5083. This Al alloy was selected because of its machinability[5] and the requirement to dissolve it after completing the TPF stage.

Samples from two different grades of Al 5083 blanks with different grain sizes were machined on a KERN HSPC 2216 micro-machining centre. The factors affecting the performance of µMilling operations investigated in a previous study[6] were taken into account in selecting the machining parameters for producing the Al master. This included (i) the selection of cutting depth that would keep milling forces within predefined limits along the machining path; and (ii) spindle speeds and feed rates were optimised for the workpiece – the cutting tool - material combination. The used machining parameters were as follows: feed rate 250 mm/min; spindle speed 40,000 rpm; depth of cut 2 µm; and step over 50µm. The channels and reservoirs were machined to their full depth of 150 µm by applying

reciprocating plunge-cut cycles. A 150 μm nominal diameter end-mill was used to mill the channels and the reservoirs.

2.4 TPF of BMG inserts

A hot embossing machine based on a Zwick universal testing machine with short cycle times was employed to produce the Zr-based BMG master. For each trial, a circular/ rectangular flat Vit 1b workpiece having a diameter/ side lengths of 15mm with an approximate thickness of 2mm was placed together with the Al master between parallel heated compression platens. The workpiece and Al master combination was then heated to a temperature above the Vit1b Tg, and then a pre-defined pressure was applied over a set time. After that, the load was gradually removed and the Al master-BMG insert "sandwiched" structure was cooled down.

To fill completely the Al master micro features it is essential to select a high processing temperature as the viscosity of the BMG decreases dramatically as the temperature increases. However, it is important to stress that after a certain time at a given temperature above Tg, the Zr-based BMG will start crystallising. Thus, the material morphology should also be controlled because it affects the Vit1b homogeneity, and consequently, it will have a negative effect on the Vit1b's machining response to the FIB process. Therefore, it is very important to choose a temperature setting as high as possible for the respective processing time in order to maximise formability[4,7] whilst simultaneously controlling the material morphology. All these factors need to be considered in selecting the TPF process windows, given that an important objective for the HE trials was to control and maintain the Vit1b's morphology while achieving high replication fidelity with regards to micro mixer feature widths, depths and shape.

As the focus of this research was to investigate the TPF process's replication constraints with regards to the achievable replication quality for both partially crystallised and fully amorphous workpieces, a systematic optimisation of the process was outside its scope. Consequently, only five tests were carried out with different processing temperatures, applied forces and overall process times that depended on the set temperature and cooling water flow rate. The parameter settings for each of these trials are presented in Table 1. These process settings were selected based on the available Vit 1b data, experimental investigations reported in literature[4,7–9] and the specific micro-mixer test structure.

Table 1. Process Settings for the TPF Trials

Trial No / Parameters	1	2	3	4	5
Processing temp – T_p [^oC]	435	420	440	440	450
Applied Force F_p [N]	4000	6000	4000	5000	5000
Overall Process Time - t_p [s]	180	185	340	198	230

Following the embossing stage, the Vit 1b inserts were separated from the Al masters by dissolving it in a heated NaOH bath. The BMG inserts were then inspected using SEM to select the inserts with the best feature resolution and surface integrity to undergo the follow up FIB structuring and subsequent injection moulding trials. Prior to FIB structuring, the selected Vit 1b inserts were also machined by wire EDM to the required overall size to integrate them into an injection moulding tool.

2.5 FIB processing

Two inserts, one partially crystallised and one fully amorphous Vit 1b metallic glass were each FIB milled with the three grating structures in Figure 3, in order to evaluate their

machining response and thus to determine whether there are any differences in the achievable feature resolution and surface integrity. The three structures were machined onto the BMG workpieces using a Carl Zeiss XB 1540 FIB/SEM system that combines a gallium ion beam with an electron beam column. Given that the three gratings represent a 2D image composed of black and white fields/pixels, the bitmap file of this pattern was used directly by the FIB system's built-in software to control the milling operation. The depth and accuracy of the structures fabricated by FIB milling are determined by the processing parameters used. In this research, the process was set up by conducting the necessary machining trials on a fully amorphous workpiece to find out quickly a suitable processing window, whilst also achieving the best trade-offs between machining time and resulting surface quality. Both inserts were milled using the same set of process parameters in order to compare their FIB machining response. The processing parameters used in this experimental study are provided in Table 2.

Table 2. FIB Milling Parameters

Structure No.	**1**	**2**	**3**
Probe current	2nA	200 pA	10 pA
Accelerating voltage	30kV	30kV	30kV
Exposure time duration	489s	963s	1070s
Probe width	150nm	40nm	14 nm

2.6 Micro-injection moulding

The machine used to perform the micro injection moulding tests was a Battenfeld Microsystem 50. The BMG insert was integrated into the primary mould using a secondary insert holder as seen in Figure 4. Three commonly used materials in injection moulding, namely Polypropylene (PP), Polycarbonate (PC) and Polyamide filled with 20% Glass fibre

(PA+20%GF) were selected to conduct the replication trials. The first two materials were used to demonstrate the validity of this process chain for replicating satisfactorily both the micro and nano scale structures while the third one was primarily selected to investigate the durability of the partially crystalline BMG insert

.

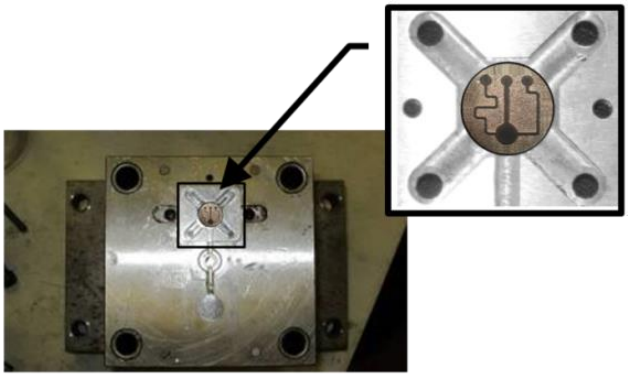

Figure 4. BMG insert and secondary insert holder assembly fitted into the primary mould

To replicate completely a mould cavity that incorporates micro and sub-micron features it is very important to select the right processing window. Many studies have been carried out to investigate how the process parameters influence the quality of the replicated parts, and the role and the consequences on the tool in achieving this [10–14] .

Since the main objective of this research was to investigate the component technologies of the proposed master making process chain an optimisation of the μIM process was not conducted and the process settings were selected based on results reported in other experimental studies.

The moulding trials were carried out in two stages. In the first stage, the process settings were selected based on the material manufacturer's data sheets and results reported in other experimental studies for PP and PC [15,16] . For both materials the initial trials showed that the process parameters needed to be optimised further in order to improve the replication quality of the nanoscale structures. Thus, the main objective of the second set of trials was to demonstrate that it was feasible to replicate nanoscale structures with a satisfactory dimensional quality. Therefore, the parameter settings were based mostly on experimental investigations into the filling performance of micro moulds with micro and sub-micrometre features reported in literature[11–14,17] , and thus to achieve as high as possible nano-scale gratings replication fidelity in terms of feature width, depth and shape. The process settings used for trials 1 and 2 for both PP and PC are presented in Table 3.

As it was mentioned above the third material was used to investigate the durability of the partially crystalline BMG insert by conducting 1000 replication cycles with a highly abrasive thermoplastic, namely PA+20%GF. The process settings given in Table 3 were selected based on the manufacturer's material data and experimental investigations reported in literature for a similar glass fibre filled polyamide[18] . In addition, the partially crystallised Vit 1b insert was specifically orientated inside the cavity so that the large reservoir was in line with the gate as depicted in Figure 4, since this was the position where maximum wear on the reservoir top edge and nano-gratings was expected.

To obtain representative results about the Vit 1b insert performance, the micro injection moulding process was first allowed to stabilise for each set of process parameter settings by producing at least 20 components and only then batches of parts were produced for quality assessment.

Table 3. Main Injection Moulding Process settings

Material:	PP (PPH 5042)		PC (Lexan HPS1-1124)		PA+GF20% (Grivory)
	Trial 1	Trial 2	Trial 1	Trial 2	Trial 1
Melt temp -- T_b (^oC)	220	240	260	290	270
Mould Temp -- T_m (^oC)	60	90	70	90	80
Holding Pressure -- P_h	ON	ON	ON	ON	ON
t_h (s)	5	8	5	8	7
Injection Speed -- V_i (mm/s)	150	200	200	400	400

2.7 Inspection

2.7.1 Dimensional measurements of microfluidic device.

All the Al and BMG masters produced by µMilling and TPF, and also five replicas selected from the batches of the PP, PC and PA +20% GF polymer parts were inspected to analyse their dimensional accuracy. The microfluidic device channel/protrusion width inspections were performed with a Leica DMLM optical measuring microscope having an integrated PixeLink camera to capture images for further digital processing using the instrument's built-in software. Whereas the depth/height of the microfluidic device channel / protrusion features were inspected using an optical coordinate measuring machine (OCMM), namely Mitutoyo QV Accel 404 Measuring System. The height/depth measurements were performed using the QV PAK software provided by the instrument manufacturer. As it was not possible to inspect exactly the same position of the channel features on the Al masters, BMG inserts' and polymer replicas' width and height/depth measurements in three predefined positions were conducted along each of the channel/ protrusion lengths and the average values were recorded.

2.7.2 Lateral measurements of grating structures.

Scanning Electron Microscope (SEM) images of the grating structures/features were taken first on the BMG inserts after the FIB milling stage and then on three PP and PC replicas to assess their lateral and vertical (XY) dimensions. These images were taken on the same system where the FIB machining was performed, in particular the Carl Zeiss XB 1540 FIB/SEM system. On each sample, three measurements for each grating were conducted in both the X and Y directions to obtain their overall widths. At the same time, 10 different pixels in X and Y directions were also measured to obtain their widths and the average values are reported.

2.7.3 Depth measurements of grating structures.

The three gratings on the Vit 1b inserts, and also on three PP and PC replicas were inspected with a Park Systems XE-100 atomic force microscope (AFM) in its non-contact mode configuration. The dimensions of the scanned areas were 35 x 35 µm, 22 x 22 µm and 7 x 7 µm for the 20 X 20 µm, 12 x 12 µm and 4 x 4 µm gratings, respectively. After the measurement, the data sets were processed using Park Systems XEI Data Processing and Analysis software to obtain the average line profiles of the features at specific locations in the scanned areas. In addition, the XEI software was used to create histograms and their two peaks corresponding to the height distributions of the original and the machined surfaces were used to determine average step heights. This method for evaluating average step heights was previously validated in another study[19] .

2.7.4 Surface roughness measurement.

The surface quality of the Al masters and their Vit 1b replicas after the micromilling and TPF steps respectively was investigated. In particular, roughness measurements of the bottom/top surfaces of their 400 μm channels and protrusions respectively were performed using the Talysurf 120 L Surface Texture Measurement instrument. Furthermore, to quantitatively assess the wear of the partially crystalline Vit 1b insert after 1000 μIM cycles with PA +20% GF, the surface roughness of the top surface of the 400 μm protrusion was also measured before and after the μIM trial. The samples' evaluation lengths were chosen according to ISO 4288: 1997[20,21] . The parameter used to inspect the surface roughness was the arithmetic mean roughness (Ra) because relative heights in micro topographies are more important, especially when measuring flat surfaces[5] . The surface texture measurements obtained were analysed using the instrument's built-in software. Three measurements were conducted along the channels/protrusions' lengths to calculate the average values of their surface roughness.

2.7.5 Micro hardness measurements.

Micro-hardness indentation measurements were carried out on the as received BMG material, and the partially crystallized Vit 1b insert after the TPF process step and 1000 μIM cycles. They were conducted using a Mitutoyo MVK-H2 Hardness testing machine fitted with a Vickers micro-indenter. The applied maximum load was 500gf. For each sample, 5 indentations were performed and the average hardness values of their measurements are reported.

2.7.6 Measurement uncertainty assessment.

The linear dimensional measurements are reported with their associated expanded uncertainty, U, at 95% confidence level, which was determined by applying an established

procedure[22–24] . For the AFM, the error contributors typical of AFM instruments[18,25–27] were considered in the uncertainty budget. Whilst, the error sources for the optical measuring microscope, optical CMM and SEM were identified by applying the recommendations for such measurements[18,28–31] . In the case of the SEM, to account for the worst-case scenario the measurement uncertainty u(P) of the SEM was calculated as 3% of the measurand's average value[31] . The reported surface roughness measurements are also provided with their associated expanded uncertainty, U, at 95% confidence level that was determined by following an established procedure[21] and by adopting recommendations given for surface roughness measurements in another study[30] .

Finally, the reported hardness measurements are also provided with their associated expanded uncertainty, U, at 95% confidence level that was again determined by following an established procedure and taking into consideration recommendations given for the estimation of hardness measurement uncertainty in the ISO-GUM standard[22] .

3.0 Results and Discussion

The experimental results obtained after each process chain step are presented in this section.

3.1 Micro milling step

Seven Al masters were produced in total using two grades of AL 5083 material. In particular, the Al 5083 samples 1 to 4 had a finer grain size to those of samples 5 to 7, respectively.

3.1.1 Dimensional accuracy.

Table 4 presents the average channel widths and depths of the Al 5083, 1 to 4 and 5 to 7 masters, respectively. The measurements of the widths were taken at the top of the channels. As expected both sets of average widths and depths values concur very closely.

Table 4 also presents the average channel widths and depths of all seven Al 5083 masters. There is a consistent deviation of the channel widths from their nominal values of 200µm, 400µm and 150µm respectively and thus it can be judged that the channels were cut oversized. This deviation is significant and is in the range between 13.3 µm and 14.5 µm and could be due to: (i) not introducing sufficient compensation for the actual tool radius; (ii) spindle/tool radial runout during machining; (iii) measurement errors as the channel edges had some burrs and thus it was difficult to detect the edge location precisely.

Table 4. The Average Dimensions of the Al 5083 Masters' Micro Features.

Samples		Channel 1 (200 µm)	Channel 2 (400µm)	Channel 3 (150 µm)
1 to 4	**Width**	213.2 ± 1.7	414.4 ± 1.6	163.6 ± 1.7
1 to 4	**Depth**	156.6 ± 2.0	155.4 ± 2.6	153.1 ± 2.2
5 to 7	**Width**	213.4 ± 1.7	414.7 ± 1.7	163.8 ± 1.8
5 to 7	**Depth**	153.2 ± 2.2	153.3 ± 1.9	152.1 ± 3.4
All	**Width**	213.3 ± 1.6	414.5 ± 1.6	163.7 ± 1.7
All	**Depth**	155.1 ± 1.6	154.5 ± 1.7	152.7 ± 1.8

It can be seen in Table 4 that there is also a consistent deviation between the channel depths and their nominal values of 150µm. Again, some systematic error is present though it is not so evident, being in the range of 2.7 to 5.1 µm. This deviation is not significant and could be due to both the spindle growth and the tool axial runouts during machining. Another contributing factor can be the measurement errors associated with the automated focussing process in detecting the top and bottom surfaces of the Al 5083 masters' channels. It should

be possible to reduce both the width and depth deviations by carefully setting up the µMilling process but anyway these results are adequate taking into account the objective of this research, in particular to investigate the capabilities of the proposed master making process chain.

3.1.2 Surface roughness.

Two average surface roughness values were obtained that correspond to samples being machined from the two different grades of Al 5083 workpieces, namely Ra 0.06 ± 0.012 and 0.34 ± 0.022 µm for samples 1 to 4 and 5 to 7, respectively. The significant difference of an almost 6 times better surface roughness can be explained with the refined microstructure of the Al 5083 samples 1 to 4 that has a direct "favourable effect on the machining response" [5,32] . This surface finish can be considered adequate for TPF of the micro fluidic structures onto the BMG insert and then to add the sub-micron and nano gratings by FIB milling in the follow up step. As FLSI is targeted in this research, especially nano scale structures are to be added on top of the pre-existing micro structures, the µMilled Al 5083 masters should have the best possible surface finish. Thus, to achieve this it is important to utilise workpieces with refined microstructures, e.g. ultrafine grained (UFG) Al alloys.

As the research reported in this paper is only a pilot implementation of the proposed master making process chain, and also taking into consideration that the µMilling process and tooling set-up strategy were not fully optimised, it can be concluded that the Al 5083 masters were successfully fabricated. Collectively, it can be stated that the machining results are very promising and demonstrate that Al TPF masters with the required surface quality and dimensional accuracy can be fabricated successfully by µMilling when the right grade of Al alloys is utilised.

3.2 TPF Step

Out of the 5 TPF trials performed, due to a set-up error and machine related malfunction, only three completely filled Vit 1b masters were produced. Consequently, in the following sections, only the results for these masters are presented.

3.2.1 Dimensional analysis.

Table 5 presents the average depths/ heights and widths of the microscale features of both the Al 5083 TPF masters and their corresponding fully filled Vit 1b replicas. Comparing the average results for the protrusions' and channels' widths it is not difficult to see that for the three trials, they concur closely.

Table 5. Comparison of Average depths & Widths of Hot Embossed BMG Inserts with Corresponding Aluminium Masters.

	Aluminium Master						**Hot Embossed BMG Insert**					
	Channel 1 (200)		**Channel 2 (400)**		**Channel 3 (150)**		**Protrusion 1 (200)**		**Protrusion 2 (400)**		**Protrusion 3 (150)**	
Trial No	Width (µm)	Depth (µm)	Width (µm)	Depth (µm)	Width (µm)	Depth (µm)	Width (µm)	Depth (µm)	Width (µm)	Depth (µm)	Width (µm)	Depth (µm)
RTN 2	213.3 ± 2.4	152.0 ± 4.1	414.8 ± 1.7	150.5 ± 1.4	163.7 ± 1.9	151.0 ± 7.6	216.6± 3.9	152.1 ± 4.4	416.2 ± 1.7	151.7 ± 5.1	166.8 ± 5.6	150.7± 2.5
RTN 4	214.3 ± 1.8	151.8 ± 2.0	414.5 ± 1.9	153.8 ± 5.5	164.4 ± 2.8	154.9 ± 6.5	217.3± 2.1	151.5 ± 5.4	419.2± 2.3	149.1 ± 4.8	166.0± 1.9	151.9 ± 5.9
RTN 5	212.6 ± 1.8	151.6 ± 3.7	414.5 ± 1.7	152.3 ± 3.8	163.3 ± 2.5	152.9 ± 5.5	215.6 ± 2.2	151.7 ± 6.2	417.4 ± 1.7	151.6 ± 5.0	165.5 ± 2.9	150.8 ± 7.1

Thus, based on the data in Table 5, the percentage difference (S) values are provided in Figure 5. There is a consistent negative S trend; in particular the Vit 1b feature widths are

consistently larger than the corresponding Al master feature widths. This is as expected and is due to both measurement errors and the dimensional changes of the Al 5083 master / Vit 1b insert micro scale features caused by the expansion/shrinkage effects of the heating/cooling cycles during the TPF step. Also, it is not difficult to see that for the three trials there is a tendency for the S values to decrease with an increase of the protrusion width, especially the 150μm protrusion 3 has the highest S value with a maximum difference of 1.9%.

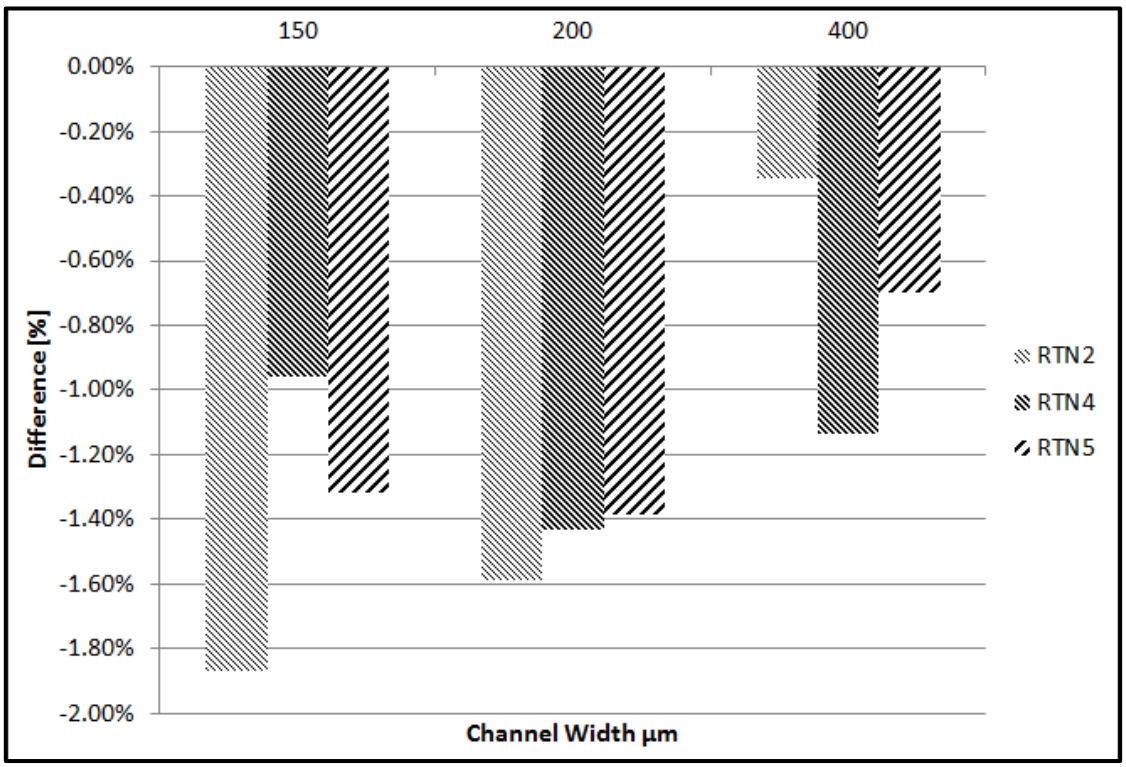

Figure 5. The percentage difference between the as-measured widths of the Al 5083 masters channels and Vit 1b inserts protrusions.

Nevertheless, the results for the three trials are very close and therefore the Vit 1b inserts can be considered accurate replicas of the Al 5083 masters in regards to the widths of the micro fluidics channels. The deviations from the pattern design is as expected, and as stated earlier they can be attributed to the expansion/shrinkage of the TPF Vit 1b insert features during the TPF heating/cooling cycles and also to some extent to measurement errors. The expansion/shrinkage magnitude is influenced by the Al 5083 alloy and Vit 1b properties in combination with the applied TPF process settings. Whereas the measurement errors are due to feature edges' definition and therefore there is an accumulation of measurement errors during feature measurements after each step in the process chain.

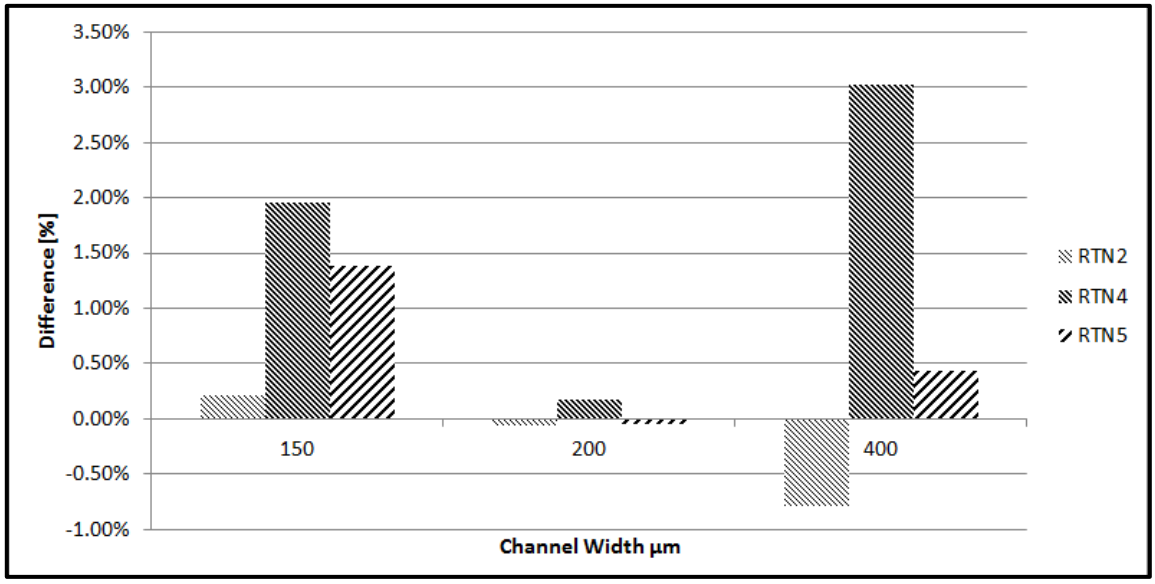

Figure 6. The percentage difference between the as-measured depths of the Al master channel features and the corresponding Vit 1b insert protrusions heights

From Table 5 and Figure 6, it is evident that that the average heights of the Vit 1b protrusions concur with the corresponding Al 5083 masters' channel depths. The negative and positive values indicate that the Vit 1b insert features are respectively larger or smaller than their corresponding Al master features. Again, they can be explained by the expansion/

shrinkage during the TPF heating/cooling cycles and the errors' accumulation when measuring the channel depths and protrusion heights of the Al 5083 masters and Vit 1b inserts, respectively. Another contributing factor to these deviations is the focusing error during the QV system measurements.

Overall it is evident from the results that the TPF performance is adequate considering the small number of trials, only three, and the specific length scales.

3.2.2 Surface quality and XRD analysis of Vit 1b inserts.

Before proceeding to the FIB milling step, it is necessary to ascertain that: (i) the material has remained amorphous or has partially crystallised after the TPF step and (ii) the surface roughness is sufficiently low such that the FIB milling can be performed satisfactorily. Therefore, the surface integrity of the embossed features was investigated using the SEM and Talysurf 120L. At the same time X-ray diffraction was used to confirm the amorphicity or otherwise of the Vit 1b inserts both before and after the TPF step.

The roughness measurements of the 400 μm channels and protrusions of the Al 5083 and Vit 1b samples used in each TPF trial are provided in Table 6. In addition, the SEM images of one as-received Vit 1b plate and the three Vit 1b inserts after the TPF trials are shown in Figure 7.

Table 6. Comparison of 400 μm Protrusions'/ Channels' Surface Roughness of Vit 1b Inserts with their Corresponding Al 5083 Masters.

	Al 5083 Master Channel 2	**Vit 1b Insert Protrusion 2**
Trial No	(Ra) (μm)	(Ra) (μm)

RTN 2	0.0752± 0.0053	0.4478± 0.0117
RTN 4	0.3490± 0.0505	0.4953± 0.0167
RTN 5	0.3378± 0.0565	0.2866 ± 0.0096

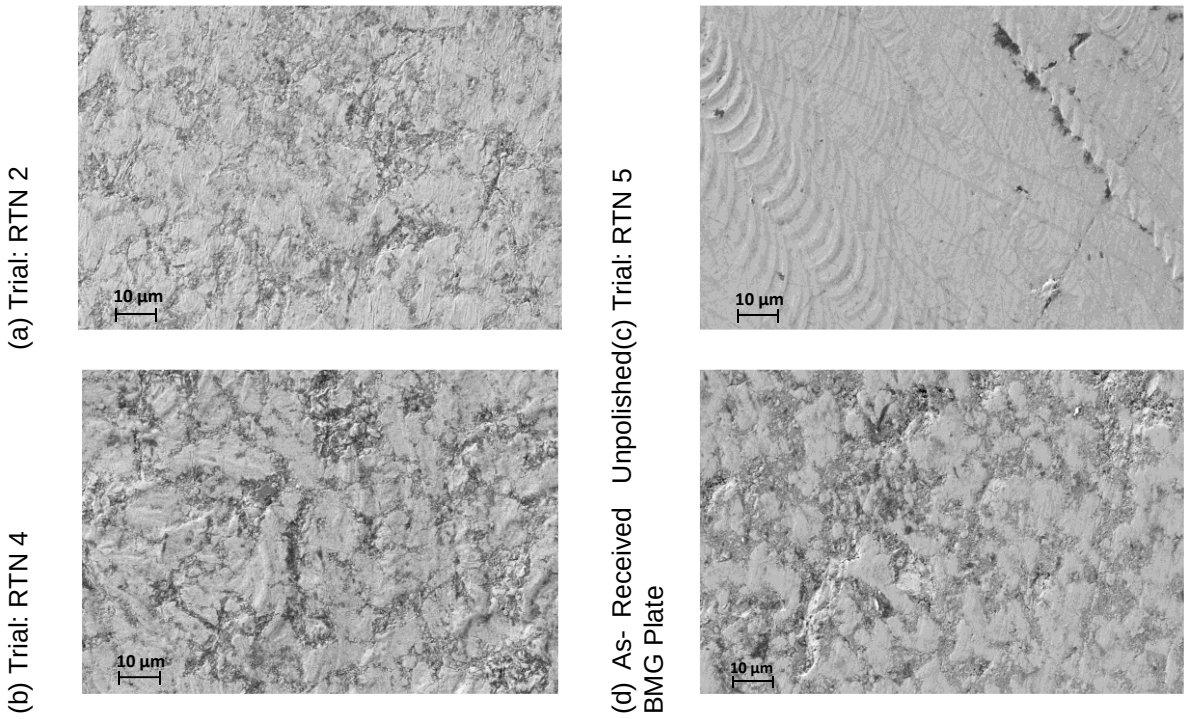

Figure 7: SEM images of the Vit 1b inserts after TPF and as received unpolished BMG plate

An initial examination of the results in Table 6 and Figure 7 reveals that the surface roughness of RTN 2 and 4 inserts are substantially higher than that of the RTN 5 insert. As it is discussed in the following section, this high surface roughness appears to originate from some initial surface contamination of the as-received Vit 1b workpieces prior to the TPF step. In particular, in the RTN 2 & 4 trials an as-received unpolished BMG plate was used,

whilst in RTN 5 it a polished one was used. Quantitatively, the average Ra values of the unpolished and polished Vit 1b plates before the TPF step were 0.48 and 0.01 μm respectively.

Analysing the results in Table 6 and the images in Figure 7 (a) and (b) and Figure 7 d) it is clear that both the Al masters' and the as-received Vit 1b plates' roughness contribute to the resulting surface roughness after the TPF step. In particular, it can be seen that for RTN 2 the surface roughness after the TPF step is marginally better than that of the as-received unpolished Vit 1b plate. Whilst for RTN 4 it is slightly worse than the roughness of the unpolished Vit 1b plate before the TPF step. Overall, these results demonstrate that the TPF process did not reduce the surface imperfections on the as-received Vit 1b plates.

These results were not expected, since a recent study[33] revealed that the TPF surfaces are two orders of magnitude smoother than the polished surface of the same alloy. Thus, the TPF process is capable of generating atomically smooth surfaces and also to replicate closely the surface topography of the Al masters. A potential contamination of the as-received Vit 1b plates prior to the TPF step together with the used embossing process settings could explain the outcomes of RTN 2 and 4. Therefore, an Energy Dispersive Spectroscopy (EDS) analysis of the as received unpolished and polished Vit 1b plates was carried out. The EDS analysis showed that the unpolished Vit 1b plates in addition to a large amount of Vit 1b elements also contain traces of aluminium and oxygen. Whilst for the polished plate these traces are substantially smaller. These results confirmed the hypothesis for a prior contamination of the as-received unpolished BMG plates with aluminium oxide (alumina) that was substantially reduced by mechanically polishing them. The alumina traces cannot be TPF at the applied embossing temperature settings and this explains the resultant high surface roughness. Such surface contamination could have originated from the Vit 1b casting process. A similar problem was reported by Bardt and Sawyer[34] where a crystalline layer was found at the interface between a silicon mould and a Zr-based BMG component.

Collectively, the results and the discussion above stipulate that although the surface roughness of the as-cast Vit 1b plates are relatively low, they still need to be polished prior to the TPF step in order to remove any surface contaminants, and thus to assure excellent imprintability at the applied embossing temperature settings.

Regarding the applied TPF processing settings, the analysis of Figures 7 a) and 7 b) shows that the µMilling texturing of the Al masters is not evident on the Vit 1b insert in RTN 2 when it is compared with the insert in RTN 4. This can be explained by the applied process settings, especially the higher embossing temperature, 440 ^{o}C in comparison with 425 ^{o}C in RTN 2. A further increase of the embossing temperature to 450 ^{o}C together with the use of the polished plate in RTN 5 led to a much clearer replication of the µMilling texturing onto the Vit 1b insert and also the insert roughness is marginally better, Ra 0.29 µm than Ra 0.34 µm on the corresponding Al 5083 master (see Table 6 and Figure 7 (c)).

These improvements in the replication performance can be attributed clearly to the lowering of the Vit 1b viscosity with the increase of the embossing temperature, and thus to facilitate the Vit 1b viscous flow and reproduce fully the surface texture of the Al master.

This is as expected since the 'viscosity' of BMG decreases dramatically as the temperature increases, and also concurs with other studies which suggest that, selecting a temperature as high as possible[4,7] whilst simultaneously controlling the material morphology is the most important consideration in identifying the optimum TPF processing window.

It can be stated that with the use of polished Vit 1b plates and proper TPF process settings it is possible to replicate accurately the Al master's surface topography even at nano scale , as the results in RTN 5 showed. The entire top surface of the Vit 1b insert's microfluidic pattern cannot be used for follow-up sub-micron and nano structuring, however adequately smooth areas can be located to carry out FIB milling. The TPF results are encouraging but they also

show that further work is required to optimise the embossing process, and thus to improve both the surface integrity and the replication quality of the produced Vit 1b inserts. The analysis of the TPF step also shows that the results can be affected significantly by the outcomes of the preceding stages in the process chain, in particular the µMilling step and also by the cross-contamination of the as-received BMG material.

The BMG inserts were analysed both before and after the TPF step to verify either their amorphicity or partial crystallinity. In particular, one as-received BMG plate and the unstructured bottom surface of each Vit 1b insert after TPF was polished and subsequently analysed by X-ray diffraction. Figure 8 depicts the XRD patterns of one as-received polished BMG plate before the TPF step, and the three Vit 1b samples after the TPF step.

In Figure 8 d) the broad diffraction maxima of the XRD spectra shows typical amorphous characteristics that are similar to those obtained for a fully amorphous Vit 1b in another study[9] and thus can be used to validate the TPF step.

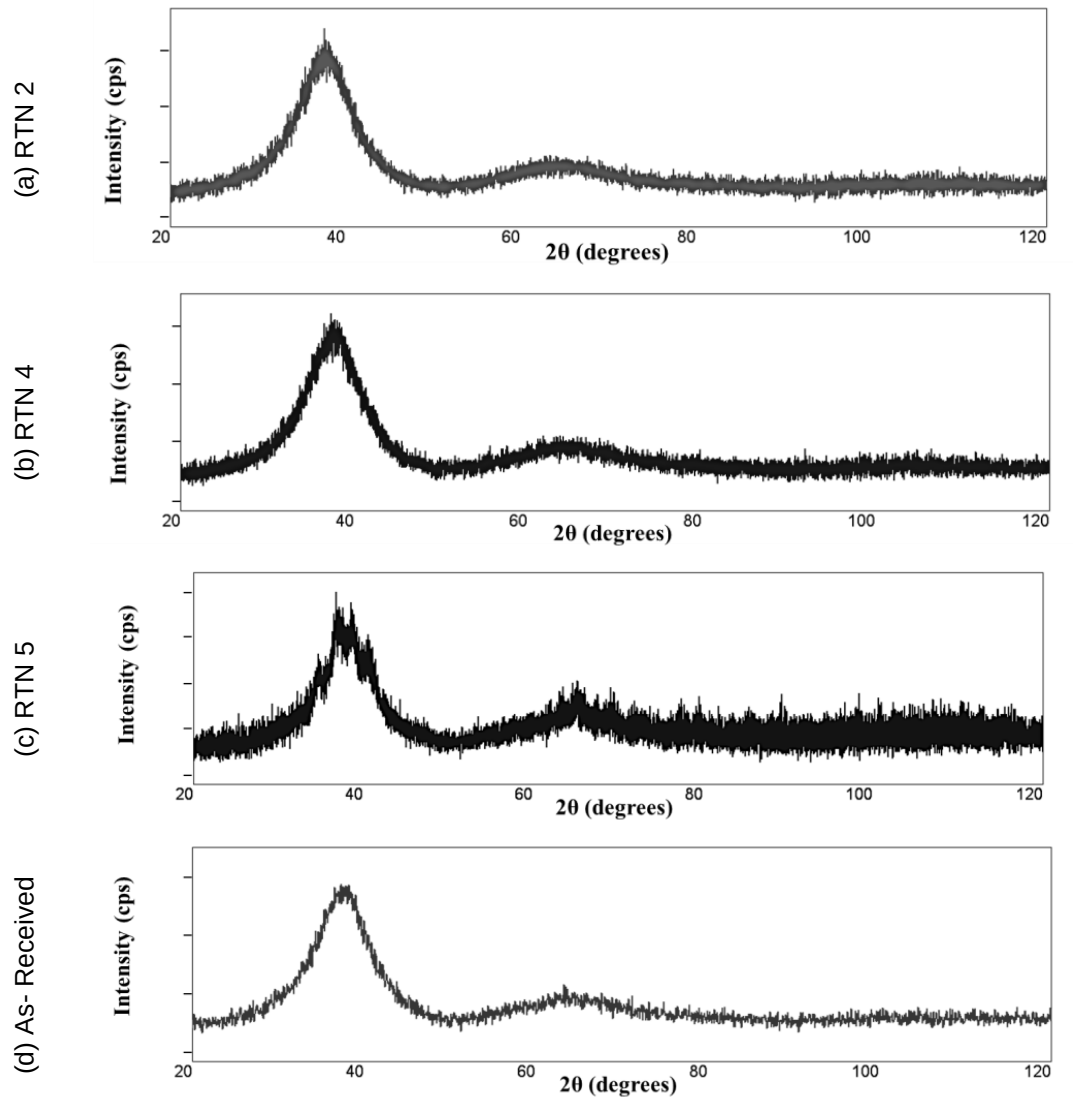

Figure 8. XRD analysis of the BMG inserts after the HE Step and the polished as received Vit 1b plate

In Figures 8 a) and b), the typical broad diffraction maxima of the XRD patterns also confirms the fully amorphous characteristics of the Vit 1b inserts in RTN 2 and 4. For both inserts, no crystalline peaks were found within the XRD detection limit and thus their amorphicity was retained at the respective TPF parameter settings. However in Figure 8 c) for RTN 5 it can be seen that there are a few weak but sharp crystalline peaks superimposed on the broad humps meaning that the full amorphicity was not retained at the respective TPF

settings and elapsed processing time. Nonetheless, since the produced Vit 1b insert is still predominantly amorphous, it is possible to create nanoscale gratings onto the top of pre-existing functional micro structures during the FIB milling step.

This partial crystallisation was not expected at the used processing conditions since the processing temperature and time were within the processing constraints discussed earlier, in particular the embossing temperature and time have not exceeded the crystallisation thresholds of 460^{o} C and 255 s, respectively [9] . This can be attributed to a combination of two factors, a lower Tx for the Vit 1b plates used that is close to the embossing temperature together with a likely shorter crystallisation onset time.

It is apparent from these XRD results that TPF is a highly sensitive but “tuneable” process and that with judicious selection of the process settings it is possible to generate both fully amorphous and/or partially crystallised BMG inserts. It is also clear that although the XRD results are within the technical requirements for producing such functional structures further improvements are possible by optimising the TPF process, especially the embossing temperature and time.

Collectively, in spite of the limited optimisation efforts in this study these results are encouraging and demonstrate that both fully amorphous and partially crystallised Vit 1b inserts with the required resolution and surface integrity can be produced by TPF.

3.3 FIB Milling Step

The partially crystallised Vit 1b insert produced in RTN 5 had the required surface quality on the reservoir surface to carry out the follow up FIB milling step. The results are compared with the same grating structures FIB milled onto a polished as-received fully amorphous Vit 1b blank.

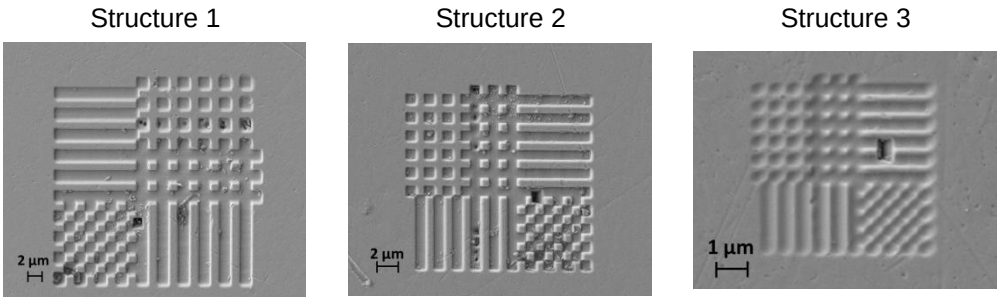

Figure. 9 Nano-scale gratings FIB milled onto a fully amorphous Vit 1b insert

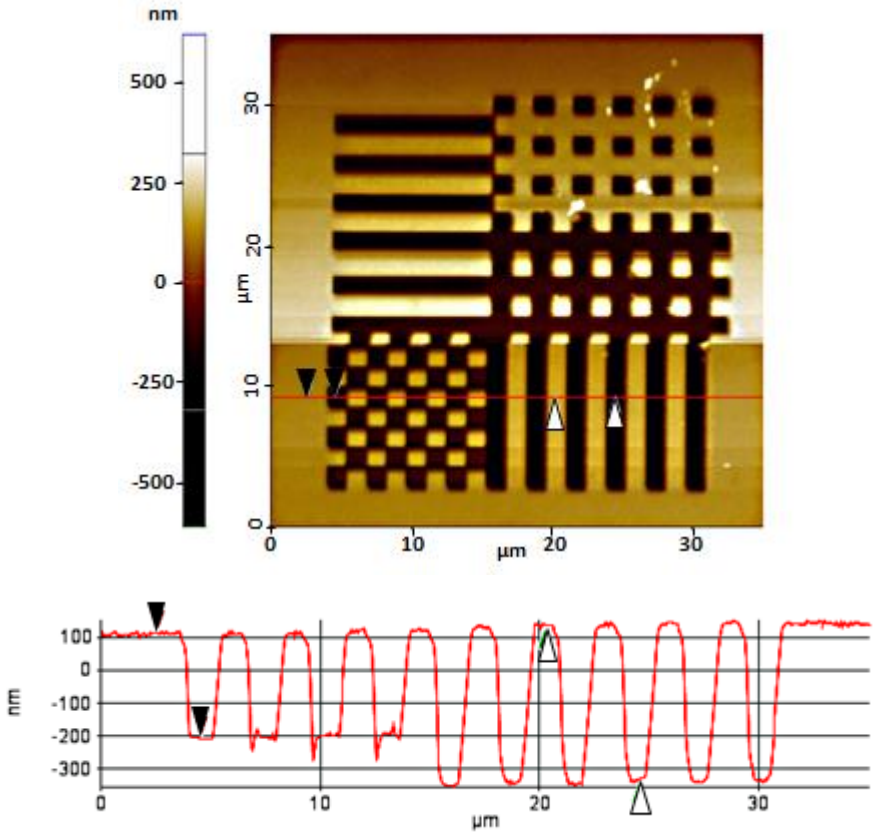

Cursor		ΔY (nm)
■	Black	-319.826
□	White	-465.199

Figure 10 Grating structure 1 profile of the fully amorphous BMG insert

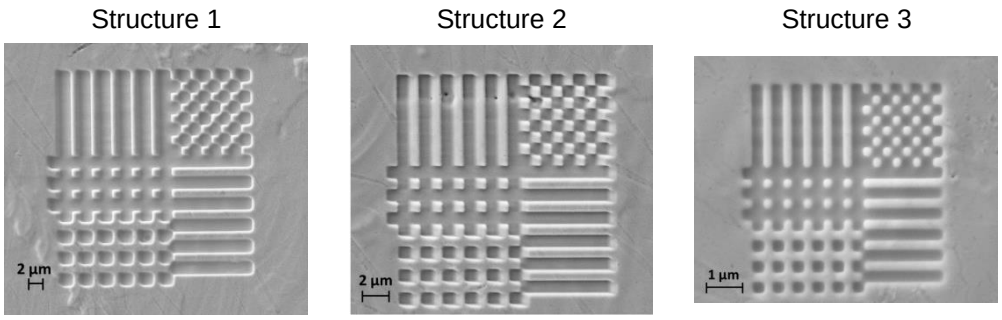

Figure. 11 Nano-scale gratings FIB Milled onto partially crystallised Vit 1b insert.

Figures 9 and 11 depict the three nano scale gratings milled onto the fully amorphous and partially crystallised Vit 1 B inserts. Comparing the images, it can be judged that for all the three grating structures, the pixel features milled on both inserts are well produced and very similar in terms of resolution and surface integrity.

The average AFM line profiles of the three grating structures at pre-defined locations were analysed. In particular, Figures 10 and 12 depict the average AFM line profiles of the 20µm gratings on the fully amorphous and partially crystallised Vit 1b inserts, respectively. It can be observed that although the same FIB parameters were used on both inserts, the pixel structures on the partially crystallised BMG exhibit a higher degree of sidewall tapering. Similar results were also observed for grating structure 2, whilst for grating structure 3 both inserts exhibited the same degree of pixel sidewall tapering.

The tapering of grating structures 1 and 2 could be explained with the used FIB process parameters that were not optimised for processing partially crystallised Vit 1b BMG substrates [35] or possibly some setting up issues as the processing of the fully amorphous sample was carried out with different system calibration. It should be noted that such tapering could be even beneficial for replicating sub-micron structures.

Tables 7 and 8 present the average heights and widths of the gratings' smallest features of both inserts, respectively. The average step heights of the pixels were determined using the histo-distributions generated from the AFM height measurements of the gratings. The tables also include the average values of the gratings' overall sizes.

Table 7. The gratings dimensions of the fully amorphous Vit 1b insert

Grating Structure No.	Pixel Protrusion Width (µm)		Protrusion Height (nm)	Overall Width (X) (µm)	Overall Width (Y) (µm)
	X	Y			
1 (20µm)	1.46 ± 0.10	1.46 ± 0.10	381.18 ± 4.6	28.83 ± 1.73	28.95 ± 1.75
2 (12µm)	0.87 ± 0.05	0.87 ± 0.06	319.73 ± 4.4	17.34 ± 1.04	17.31 ± 1.04
3 (4µm)	0.30 ± 0.03	0.31 ± 0.04	84.30 ± 4.0	5.84 ± 0.35	5.88 ± 0.36

Table 8. The gratings dimensions of partially crystalline Vit 1b insert

Grating Structure No.	Pixel Protrusion Width (µm)		Protrusion Height (nm)	Overall Width (X) (µm)	Overall Width (Y) (µm)
	X	Y			
1 (20µm)	1.46 ± 0.11	1.47 ± 0.11	461.90 ± 9.4	28.53 ± 1.72	28.59 ± 1.72

2 (12μm)	0.88 ± 0.06	0.88 ± 0.05	289.22 ± 5.7	17.26 ± 1.04	17.35 ± 1.05
3 (4μm)	0.28 ± 0.02	0.29 ± 0.03	92.03 ± 4.1	5.62 ± 0.34	5.78 ± 0.35

The comparison of the lateral dimensions shows that the values for both workpieces concur very closely. Also, it can be observed for both inserts that the average pixel widths in the X and Y directions at the bottom of the protrusions are larger than their nominal values of 1 μm, 600nm and 200nm. This difference could be due to not introducing adequate compensation for the used FIB diameters of 150nm, 40nm and 14nm, respectively and also due to measurement errors as the pixels' edges are rounded thus making their precise detection more difficult. Besides these two factors the discrepancies could also be the result of calibration and set-up issues associated with the FIB system used.

From Tables 7 and 8 it is also evident that that the average step heights of the gratings milled on the fully amorphous Vit 1b workpiece do not concur so closely with those milled on the partially crystallised counterpart. In particular, the average step height deviations are approximately 80.72 nm, -30.51 nm, and 7.73nm for the 20μm, 12μm and 4μm gratings, respectively. At this point, taking into account the limited number of inserts and the inconsistencies of these small deviations, it is not possible to state unequivocally if they are significant and due to differences in the milling FIB response of the two inserts or whether they may be attributed to stochastic factors.

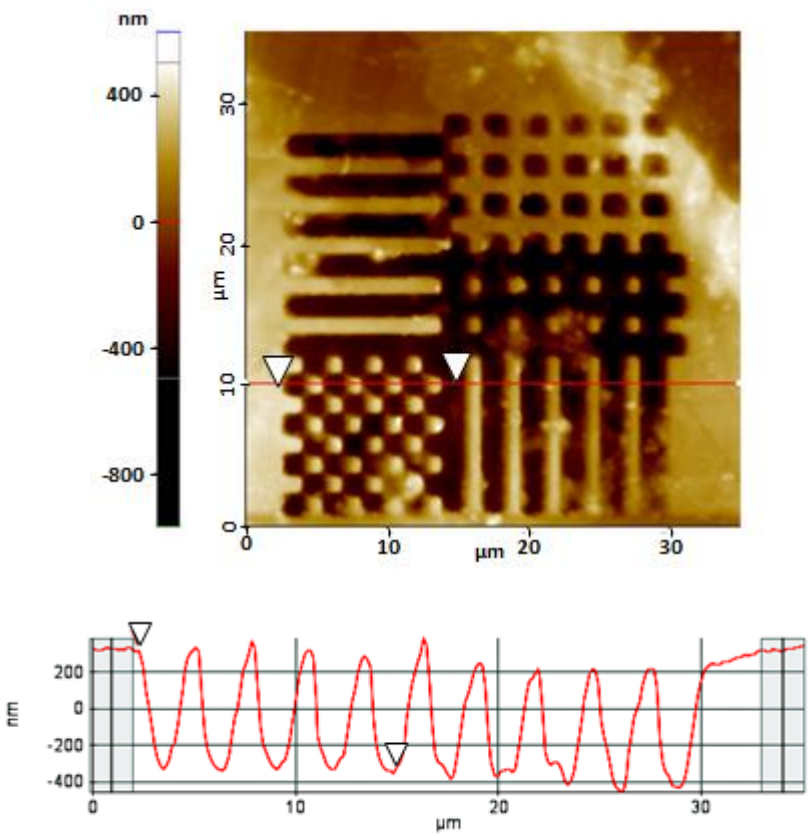

Cursor	ΔY(nm)
White	-643.564

Figure 12 Partially crystallised grating structure 1 profile of the features

The step height results for the three grating structures also show that for both inserts the average heights are substantially smaller than their nominal values of 1 µm, 600nm and 200nm, respectively. In addition, examining Figures 10 and 12 it can also be judged that the FIB milling depths are also not uniform across the grating structure 1 on both inserts. Similar results were obtained for the other two gratings. Again, these results could be explained both with the measurement errors associated with the quality of the pixel edges and also with not properly calibrating the layer-based FIB milling process, in particular the sputtering rates for the selected FIB milling settings in Table 2. If such a calibration is carried out the form

deviations of complex 3D structures could be kept within 2 to 5 % of their nominal dimensions[31] .

In spite of the limited optimisation efforts, the results show that the geometrical accuracy and surface integrity of the nano-scale grating features on the partially crystallised Vit 1b insert are similar to those obtained on the fully amorphous workpiece. There were some deviations from the nominal dimensions and shape but the FIB milling process can be optimised to meet the requirements of the proposed FLSI enabling master making process chain.

3.4 µIM process step

3.4.1 Replication of microfluidic device pattern.

Figure 13 shows the microfluidic device pattern (see Figure 2) that was replicated well using the three materials, PP, PC and PA+20% GF, investigated in this research.

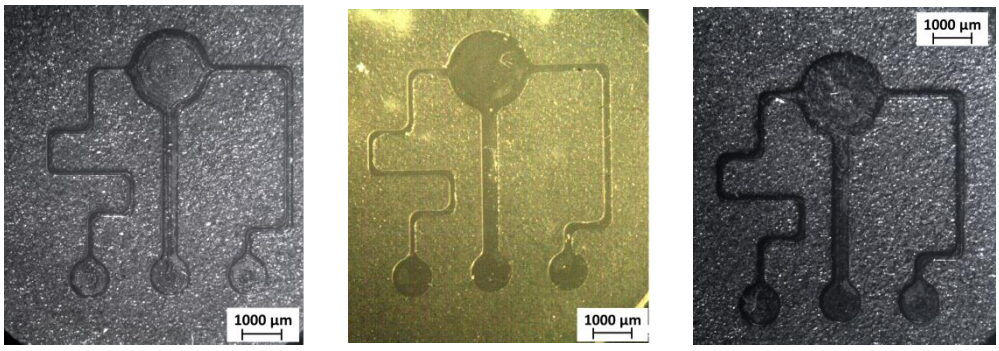

a) PP Microfluidic Device. b) PC Microfluidic Device c) PA+20% GF Microfluidic Device.

Figure 13. Replicated microfluidic patterns in PP, PC and PA+20% GF

The average channel heights and widths of the PP, PC and PA+20%GF micro-mixer replicas generated using the Trial 1 process parameter settings (see Table 3) are provided in Table 9.

Comparing the partially crystallised RTN 5 insert's average protrusion width in Table 5 with the corresponding channel width of the replicas in Table 9, it can be judged that they concur closely.

Table 9. The Dimensions of Replicated Microfluidic Devices

Trial No	**Channel 1 (200)**		**Channel 2 (400)**		**Channel 3 (150)**	
	Width (µm)	Depth (µm)	Width (µm)	Depth (µm)	Width (µm)	Depth (µm)
PP Parts	203.5± 2.1	148.0± 1.7	404.2± 2.1	148.2± 1.6	153.7 ± 2.4	147.4± 1.3
PC Parts	211.6± 2.8	149.7± 1.6	414.9± 2.6	150.2± 1.6	158.9± 2.4	149.4± 2.0
PA + 20%GF Parts	212.1± 2.9	150.3± 2.2	414.3± 2.1	149.9± 2.4	157.2± 2.9	150.7± 2.3

The average percentage difference for the channels is around 5.3%, 2.1 % and 2.5% for the PP, PC and PA + 20% GF materials respectively. These deviations are higher than the expected typical shrinkage values of 1 to 2% for PP, 0.5 to 0.7 % PC and 0.15 to 0.75 % for the PA+20% GF. Again, measurement errors due to not well defined channel and protrusion edges together with the used injection moulding parameters, in particular the packing pressure and time, could be the reasons for this. PP parts exhibit the highest percentage difference, which can be attributed to the cooling rates that affect the shrinkage of a semi crystalline material. In particular, the mould temperature was set towards the maximum recommended value in order to replicate fully the sub-micron structures. However, this caused the PP replicas to cool down more slowly and led to a higher crystallinity and shrinkage[36,37] . This problem can be overcome by increasing the cooling rate and consequently the shrinkage can be reduced. As expected the average shrinkages of PC and the glass filled PA replicas are significantly lower than that of the PP replicas. In particular, they are more accurate replicas of the BMG insert's microfluidic pattern with

average width deviations of 2.1 % and 2.5 %, respectively. Again, a higher than typical shrinkage of the glass filled PA replicas can be explained with the material's semi crystallinity, however, the negative effects are mitigated by the presence of glass fibres.

The insert's protrusion height (see Table 5) concurs quite closely with the corresponding channel depths of the replicas in Table 9. The average difference for all channels is around 2.3%; 1.04 % and 0.70% for the PP, PC and PA + 20% GF replicas, respectively. As expected, this difference is less than that for the channel widths because the shrinkage is higher in the direction of the polymer flow[37] . However, the differences are again small and therefore all the polymer parts can be considered accurate replicas of the BMG insert microfluidic pattern despite the fact that the process parameters were not fully optimised.

3.4.2 Replication of nano-scale gratings.

Figure 14 shows that the grating structures were replicated successfully on the polymer parts when using the fully amorphous Vit 1b mould insert and the Trial 2 µIM parameter settings in Table 3. There are some localised voids in the grating structures on both the PP and PC replicas due to some trapped air in the microcavity. This can be minimised by introducing air evacuation from the cavity prior to injection[13,38–40] and thus to improve further the replication quality of the nanoscale structures.

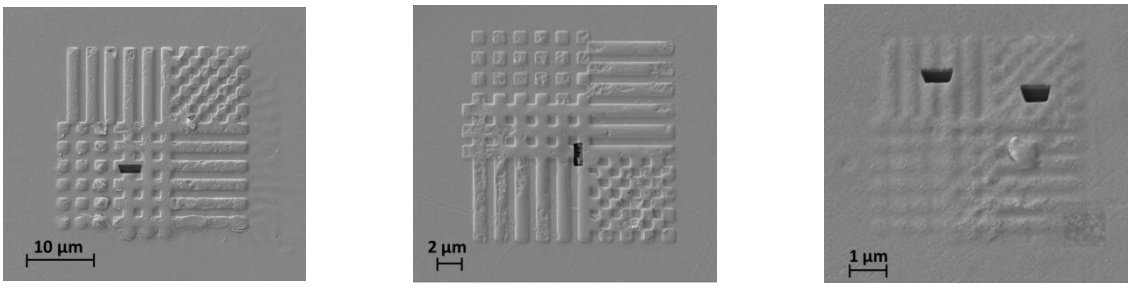

a) PP Structure 1 b) PC Structure 2 c) PP Structure 3

Figure 14. Replicated grating structures**.**

Tables 10 and 11 show the average heights and widths of the smallest gratings' features from the samples replicated in PP and PC, respectively. Also, the tables show the average overall sizes of the gratings in the X & Y directions. The dimensions of the three gratings concur closely with the corresponding ones in Table 7 for the fully amorphous Vit 1b insert. In particular, the pixel width deviations vary between 0.7 to - 6.3 % and 0 to -3.5 % for the PP and PC replicas, respectively, but there is no consistent percentage difference trend. The average width dimensions of the "small" pixels were also calculated based on the overall sizes of the individual gratings in Tables 7, 10 and 11 and the number of pixels (20) in order to minimise the effects of the accumulated measurement errors associated with the quality of the "pixel" edges. If the shrinkage is calculated based on these more realistic width values the differences are reduced to 2.1 - 3.3 % and 0.9 - 2.6 % for the PP and PC replicas, respectively. For both polymers, these deviations are still higher than the expected typical shrinkage values and again they can be explained with the injection moulding settings that were not fully optimised and also the semi crystallinity in the case of PP.

Table 10. PP Gratings Micro and Nano - scale Feature Dimensions

Grating Structure No.	Pixel Protrusion Width (μm))		Protrusion Height (nm)	Overall Grating Structure Width (X) (μm)	Overall Grating Structure Width (Y) (μm)
	X	Y			
1 (20μm)	1.46 ± 0.10	1.45 ± 0.09	369.02 ± 8.2	28.32 ± 1.70	28.30 ± 1.70
2 (12μm)	0.91 ± 0.06	0.92 ± 0.07	306.23 ± 6.7	16.86 ± 1.01	16.97 ± 1.02
3 (4μm)	0.32 ± 0.03	0.32 ± 0.03	74.72 ± 4.1	5.65 ± 0.34	5.74 ± 0.35

Table 11. PC Gratings Micro and Nano - scale Feature Dimensions

Grating Structure No.	Pixel Protrusion Width (μm))		Protrusion Height (nm)	Overall Grating Structure Width (X) (μm)	Overall Grating Structure Width (Y) (μm)
	X	Y			
1 (20μm)	1.5 ± 0.09	1.5 ± 0.10	360.50 ± 11.7	28.72 ± 1.73	28.67 ± 1.72
2 (12μm)	0.90 ± 0.06	0.90 ± 0.06	316.78 ± 9.3	16.99 ± 1.02	16.91 ± 1.02
3 (4μm)	0.30 ± 0.02	0.31 ± 0.02	78.67 ± 4.2	5.70 ± 0.34	5.73 ± 0.34

The gratings' step heights of the PP and PC replicas in Tables 10 and 11 respectively were also determined by considering the histo-distributions generated from the AFM scans. Comparing them with their corresponding heights for the fully amorphous Vit 1b insert in Table 7, it can be observed that they are consistently slightly smaller. In particular, the average depth difference for all three gratings varies between 3.2 - 11.4 % and 0.9 - 6.7 % for the PP and PC parts, respectively and again they are higher than the expected typical shrinkage values due to the same reasons as those for the width deviations. Figure 15 depicts a typical average line profile of the 20μm grating replicated on one of the PP parts. The pixel depths are not uniform and similar results were obtained for the other two gratings

on the PP replicas and also for the three gratings on the PC replicas. These results can be attributed both to some non-uniformity of the gratings in the Vit 1b insert and again with some trapped air.

Thus, it can be judged that the 20µm, 12µm and 4µm gratings were replicated successfully on the PP and PC mouldings in this feasibility study but the quality can be improved further by optimising the µIM settings systematically. Also, the research has revealed potential challenges in performing an effective quality control and reliable manufacturing at sub-micron scale that should be addressed, too.

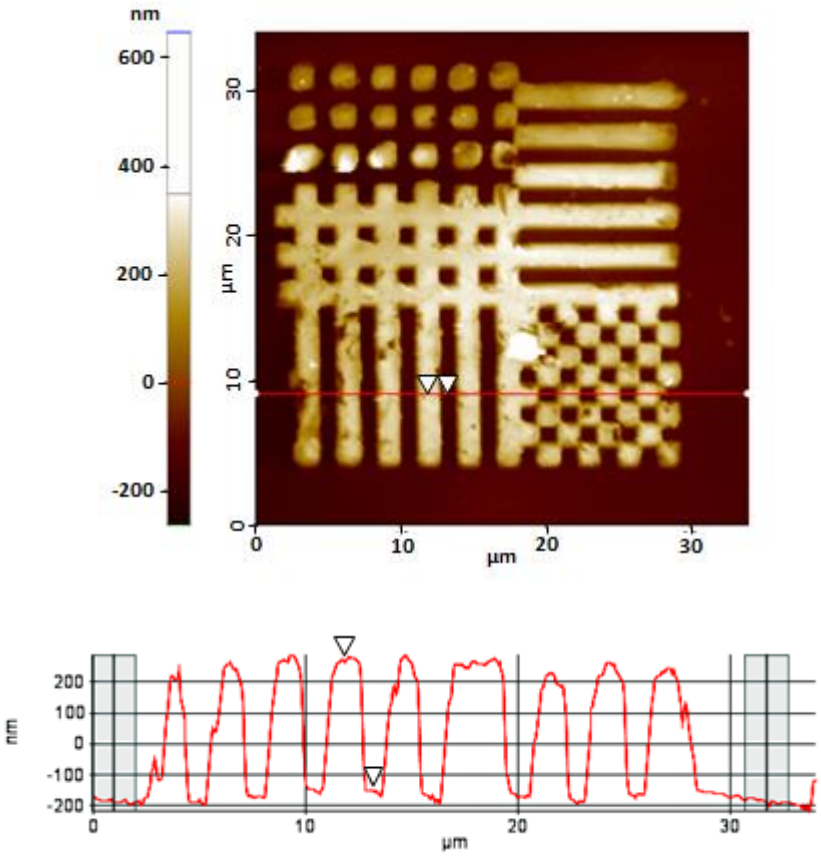

Cursor	ΔY(nm)
☐ White	-419.713

Figure 15 PP Grating structure 1 AFM profile of the features

3.4.3 Tooling Performance Evaluation.

In this section the performance of the partially crystalline BMG insert is evaluated by studying it's condition after enduring 1000 injection moulding cycles with the highly abrasive PA+20% GF thermoplastic.

Insert wear. SEM images of the Vit 1b insert's surface before and after the 1000 injection cycles are used for a qualitative wear assessment. Figure 16 shows SEM images of the large reservoir side wall in a selected location at progressively increasing magnifications: (a) before the µIM trials, 0 shots, (b) after 167 cycles and (c) after 1000 cycles. The smoothening effect on the reservoir edge and the µMilling surface texture with the increase of µIM cycles is very small in spite of fact that the imaged area was situated directly in front of the gate and as consequence of this there was some glass fibre impingement erosion. Furthermore, the glass fibres seem to leave scratches on the reservoir's top surface and upper part of the side wall due to the sustained strain during the µIM cycles. The reason for this is that the reservoir's surface is not only strained during the polymer injection step but also during the demoulding of the solidified replicas.

Figure 17 shows SEM images of the three grating structures and their surrounding areas on the large reservoir after 1000 injection cycles. Comparing Figures 11 and 17, it can be seen that the three structures show varying degrees of wear and also some plastic deformation of the pixel structures. Some indentation like marks can also be observed. Depending on the angle on impingement, the glass fibre endings seem to either leave traces of scratches when the polymer is flowing over the surface or indentation, impact or deformation marks when hitting the surface. Considering that all three gratings, especially the 4 µm one, are still relatively intact and the µMilling marks are also still clearly visible after the exposure to 1000

µIM cycles with the highly abrasive PA +20%GF thermoplastic it can be judged that the wear on these structures is relatively small.

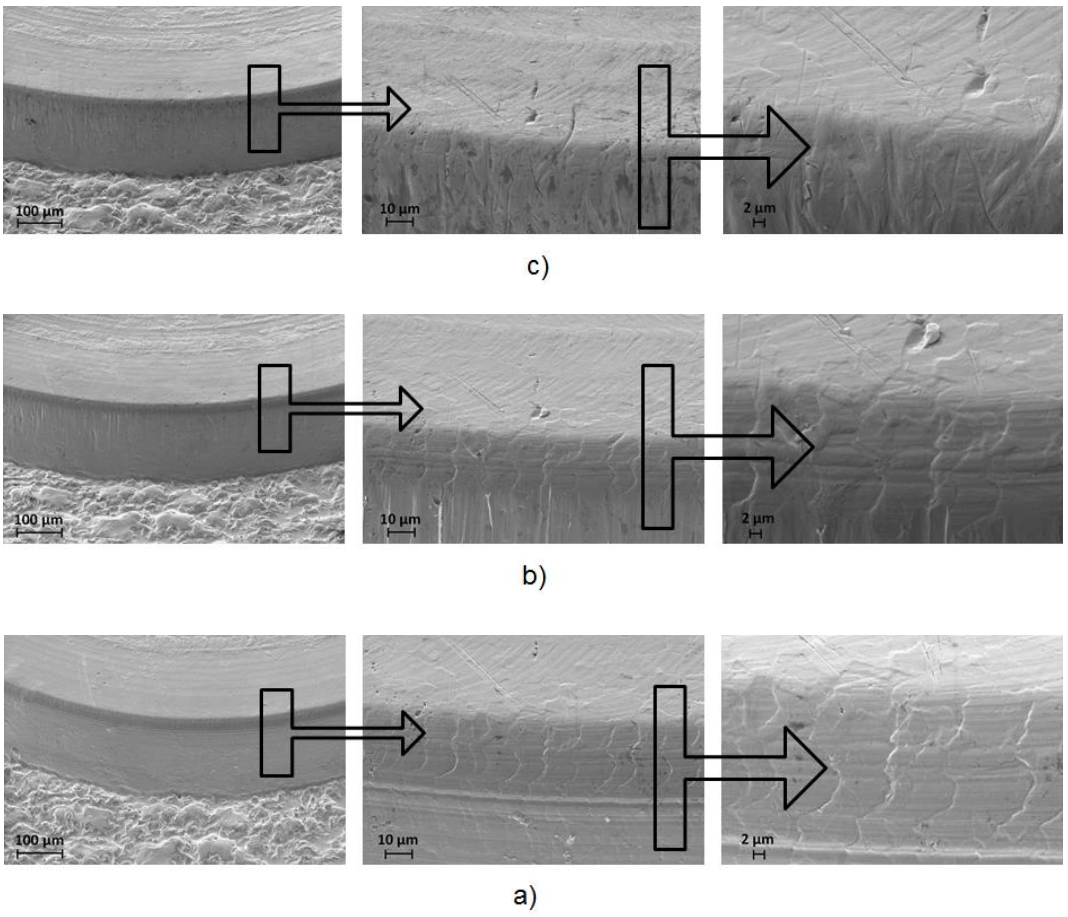

Figure 16. SEM Images of the Vit 1b insert side wall: (a) before the µIM trials, (b) after 167, and (c) 1000 injection cycles.

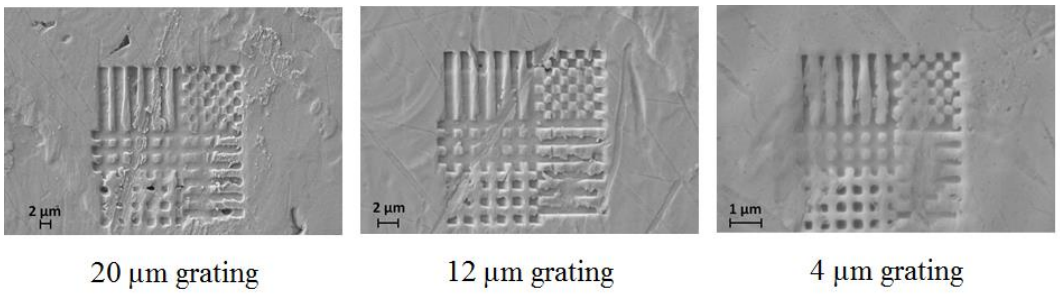

Figure 17. SEM Images of the Vit 1b insert gratings after 1000 injection cycles

The surface roughness of the 400µm protrusion before and after the 1000 µIM cycles was Ra 0.8 ± 0.02µm and 0.3 ± 0.01µm µm, respectively, which represented an increase of approximately 500 nm. Although this appears to be a significant increase, the wear effects can be considered relatively small if the aggressive abrasive conditions during the µIM cycles are taken into account, in particular the used temperature settings in combination with the e-glass's hardness that is approximately 64% higher than that of the partially crystallised Vit 1b insert. This estimation was based on the measured average Vickers micro-hardness value, Hv 597 of the partially crystallised Vit 1b insert after the TPF process step. Thus, it can be judged that the surface degradation of the Vit 1b insert is mainly due to sustained strain during the µIM cycles, in particular as a result of the inflow of the polymer and ejection of the solidified polymer parts from the mould[41] .

It is also evident that the mechanism and degree of surface degradation depend mainly on the mould geometry, the type of thermoplastic and filler material used, the volume fraction of filler materials, the filler (fibre) inclination angle, injection conditions and the response of the mould material[41,42] .

With respect to the material's response, it should be noted that there is a general correlation between the hardness and the BMGs' wear resistance[43–47] . In particular, a lower hardness produces a lower wear resistance; and also that hardness and wear resistance are both

observed to be enhanced by partial crystallization of the BMG. Therefore, the micro-hardness of the as-received and the partially crystallised Vit 1b insert after the TPF step and 1000 µIM cycles, was measured and the Vickers hardness values obtained were 534.4 ± 27.7, 596.7 ± 26.4 and 597.3 ± 27.0 HV, respectively. Similar HV micro-hardness values were reported for amorphous and fully crystallised Zr-based BMG alloys with compositions similar to that of the Vit1B alloy[48,49] . As expected the Hv values of the Vit 1b insert after the TPF process step increased by 11.7 % and remained the same after the 1000 µIM cycles, and thus the wear resistance of the partially crystallised Vit 1b should have improved, too.

The results from the carried out in-situ wear trials in combination with the results from the Hv tests are very encouraging. The wear resistance of the Vit 1b insert can be judged to be satisfactory while the introduction of the crystalline nano phases in the monolithic-amorphous Vit 1b appears to be an effective means of improving the wear resistance.

Failure mechanism. After approximately 1150 injection moulding cycles, the partially crystallised Vit 1b insert showed signs of cracking. This premature failure was not expected and therefore a further analysis of the insert was carried out to identify the probable mechanism leading to this. The Vit 1b insert was constrained within the mould base and consequently it experienced complex repeated stress cycles due to both temperature and pressure variations during the µIM trials. Thus, the insert failure could be due to material fatigue as a result of underwent dynamic and cyclic stress that led to the initiation of cracks and then their propagation and final fast fracture [50] . To confirm this, the insert's surface was examined by SEM.

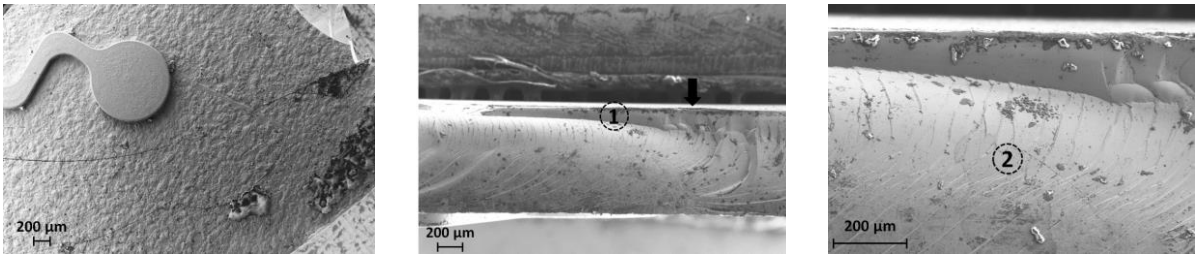

(a) A Top view of fractured BMG insert

(b) A top view of a fracture surface

(c) Region 1 at higher magnification and coarse striations in Region 2

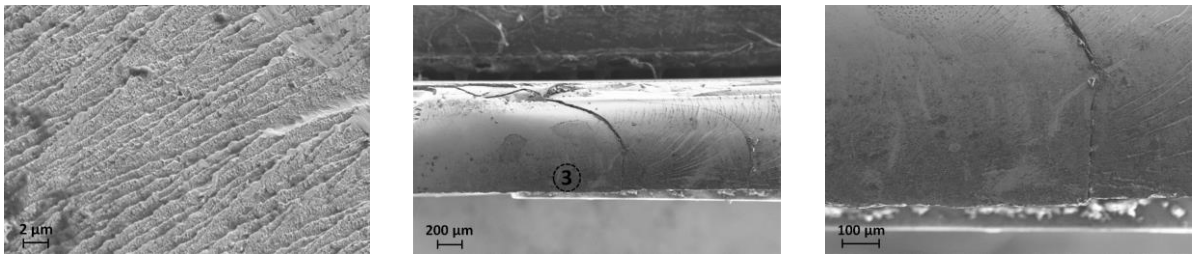

(d) Magnified image of region 2 showing fine within coarse striations

(e) Region 3

(f) Magnified Image of Region 3

Figure 18 SEM images of fractured BMG insert

Representative SEM images of the examined fractures are shown in Figures 18a to 18f. Figure 18a shows a plan view of the Vit 1b insert with various cracks running across the insert top surface while Figures 18b to 18f depict the fracture surfaces that are normal to the insert surface. Three distinct regions can be observed, namely: (i) region 1 near the top surface, where the fracture is smooth and flat (Figures 18b and 18c); (ii) region 2 exhibiting a striation-type fracture that covers most of the surface (Figures 18c and 18d); and (iii) region 3, which is very rough and demonstrates a dimple-type morphology (Figures 18e and 18f). It is evident that the µIM trials generated complex stress states and thus it is difficult to directly correlate the insert's fracture morphology with that obtained in conventional fatigue tests.

However, similar fracture morphology to that in regions 1, 2 and 3 was reported in other studies on the fatigue behaviour of both fully amorphous and partially crystallised BMGs

where their differences were associated with the crack initiation site, propagation area and final fast fracture surface respectively[51–53] . This suggests that the insert failure is caused by fatigue and the following factors could have affected the fracture mechanism: surface quality, insert size, and microstructure related effects[50,54–56] .

It should be noted that no microstructural defects were observed on the fractured surfaces. However, it can be seen in Figure 18a that the top surface of the insert is relatively rough. The fatigue behaviour is sensitive to the insert's structural quality and surface flaws/ irregularities[54,56] that can lead to stress amplification and initiation of cracks[50] . Thus, the Vit 1b surface quality after the TPF process step (the replicated µMilling texture and also the burrs), and during the µIM cycles (glass fibre induced scratches and indentations during the µIM cycles); and the potential BMG plasticity modifications due to multiple thermal processing steps could have all adversely affected the insert fatigue behaviour.

Another contributing factor could have been the relatively small size of the insert as the fatigue lifetimes and endurance limits of the large-size samples are greater[55] . Taking into consideration the limited number of experiments carried out and the contributing factors discussed above it is apparent that this fatigue issue requires further investigation.

4.0 Future Research

As it was already noted all component technologies in the proposed master-making process chain have to undergo further optimisation. Such process optimisation can be achieved either by employing specially developed methodologies such as that reported earlier for optimising the layer-based FIB milling process or through the use of the DOE methodology[57–59] .

The results reported in this paper also highlighted other areas for further research to address specific shortcomings in the proposed master making process chain. In particular, the fabrication of Al TPF masters employing the µMilling process shows real promise when an ultrafine grained Al alloys are utilised. However, it was also clear that process optimisation will not be solely sufficient to completely eliminate the burrs on the top edges of the microfluidic channels and achieve the required surface finish for the follow up FIB machining. Therefore, additional surface conditioning and post processing should be considered to eliminate the burrs and improve the surface quality after the µMilling step.

Another possible way to improve the surface quality of the Vit 1b inserts is to have some additional surface conditioning and smoothening after the TPF step. Recent research has shown that micro and nano scale features imprinted on a Pt-BMG, using TPF at a temperature above Tg can be erased by subsequent annealing at a set temperature in the material's super-cooled liquid region (SCLR)[60,61] . This phenomenon explores the mechanism of shape-recovery that is driven by surface tension viscous flow in the BMGs' SCLR and can be used as a surface smoothening process. However, such post processing step has not been investigated for achieving a similar effect on Zr-based BMGs.

The µIM process is an important means for scale up production of polymer based FLSI devices and shows real promise when air evacuation in combination with some additional process optimisation are applied. However, it was also clear that a more radical approach is necessary in overcoming the process deficiencies, e.g. by employing a compression injection moulding [27,62] in conjunction with a prior air evacuation step[13,38–40] .

The results from the carried out preliminary in-situ injection moulding trials with PA containing 20% glass fibres together with the results from the micro indentation tests are

encouraging. The introduction of crystalline nano phases in the monolithic-amorphous Vit 1b samples appears to be an effective means of improving the hardness of the material and consequently its wear resistance. However, the lifetime of the Vit 1b insert in terms of wear is still not properly verified and thus warrants a further investigation. In particular, although hardness is usually regarded as a primary material property which determines the wear resistance, the elastic modulus can also have a significant impact on wear behaviour. Therefore, a more suitable parameter for predicting wear resistance will be the ratio of hardness (H) and elastic modulus (E), rather than hardness alone[63] . In addition, the fatigue life of the Vit 1b insert after the introduction of the crystalline phase requires also some further investigation. Nanoindentation tests in conjunction with some additional XRD analysis can be employed to understand better the thermo-mechanical effects of the TPF and μIM steps on the Vit 1b workpieces in regards to their wear resistance and fatigue life.

5.0 Conclusions

This paper presents an experimental investigation of a master making process chain for achieving FLSI in devices. The research demonstrated that the process chain can be a viable fabrication route for both fully amorphous and partially crystalline Zr-based BMG inserts that incorporates different length scale features. The results show that relatively good fidelity of the different scales' features can be achieved with the μIM process and it can enable FLSI in thermoplastic components. Collectively, there is good process compatibility and complementarity between the component technologies in the process chain and thus to enable FLSI in masters and ultimately in thermoplastic replicas. In particular, the masters and/or replicas after each processing step, were analysed and the factors that are considered to have the highest impact on the overall performance of the process chain are: (i) workpiece microstructure both for producing the Al masters and then the BMG inserts; (ii) the optimisation of the set-ups and processing conditions for the component technologies;

and (iii) the Zr-based BMG response to TPF and FIB processing. In addition, the following conclusions regarding the component technologies and their contributions to the process chain overall performance were made:

- The analysis of the TPF and FIB steps shows that their results can be affected significantly by the preceding component technologies in the process chain, in particular the Al masters produced by µMilling and then both µMilling and TPF steps, respectively. Therefore, additional surface conditioning and post processing should be considered to improve the resulting surface quality after the µMilling and TPF steps.
- The analysis of the complex features' profiles revealed that the feature geometry was accurately transferred through the three steps of the master-making process chain to the Zr-based BMG insert and also that a careful selection of inspection strategies is required in order to minimise measurement uncertainty.
- The surface contamination of Zr-based BMG workpieces adversely affects the surface integrity of the inserts after the TPF step. The study has shown that it is essential to polish the as-received workpieces prior to the TPF step to eliminate any surface contamination. The use of workpieces with some surface contamination limits the replication performance of the TPF step.
- Nano-scale grating structures were successfully produced using the FIB process on both the fully amorphous Zr-based workpiece and also on micro features of a partially crystalline insert after the TPF step. In particular, the geometrical accuracy and surface integrity of the nano-scale grating features on the partially crystallised BMG insert are similar to those obtained on the fully amorphous workpiece, thus confirming that their response to FIB machining is similar.
- The analysis of thermoplastic replicas shows that the nanoscale replication results can be significantly affected by the FIB milling step and the µIM process settings.

- The in-situ wear tests in combination with the micro indentation hardness tests provided evidences that the wear resistance of the insert was improved by introducing crystalline nano phases in the monolithic-amorphous Zr-based BMG and thus the use of such inserts could extend the tool life, especially when replicating micro and sub-micron features. At the same time it should be noted that the fatigue performance of the insert can be affected significantly by the preceding stages in the master-making process chain, in particular the µMilling, and potentially the TPF and µIM steps.

Acknowledgements

The research reported in this paper was funded by the FP7 programmes ‘‘Integrating European research infrastructures for the micro-nano fabrication of functional structures and devices out of a knowledge-based multimaterials’ repertoire” (EUMINAfab) and "High throughput integrated technologies for multimaterial functional micro components" (HINMICO). The authors would like to thank also the University of Malta for the financial support of Pierre Vella’s PhD research and ERDF (Malta) for financing some of the testing equipment used in this research through the project: “Developing an Interdisciplinary Material Testing and Rapid Prototyping R&D Facility (Ref. no. 012)”

The technical assistance of the authors’ colleagues, particularly Dr Ekaterin Minev, Dr Petko Petkov, Dr Krastimir Popov, Dr Emmanuel Brousseau, Dr Matthias Worgull and Dr Stefan Scholz at Cardiff University and Karlsruhe Institute of Technology is gratefully acknowledged.

References

1. HLEG. Key Enabling Technologies -- Final report [Internet]. June 2011. European Commission; 2011. Available from: <http://ec.europa.eu/enterprise/sectors/ict/files/kets/hlg_report_final_en.pdf>

2. Dimov SS, Brousseau EB, Minev R, Bigot S. Micro- and nano-manufacturing: Challenges and opportunities. *Proc Inst Mech Eng Part C J Mech Eng Sci.* 2012;226(3):3–15.

3. Schroers BJ. Processing of Bulk Metallic Glass. *Adv Mater.* 2010;22(14):1566–1597.

4. Schroers J, Pham Q, Desai A. Thermoplastic Forming of Bulk Metallic Glass — A Technology for MEMS and Microstructure Fabrication. *J Microelectromechanical Syst.* 2007;16(2):240–247.

5. Popov KB, Dimov SS, Pham DT, Minev R, Rosochowski A, Olejnik L. Micromilling: Material Microstructure Effects. *Proc Inst Mech Eng Part B, J Eng Manuf.* 2006;220(11):1807–1813.

6. Dimov S, Pham DT, Ivanov A, Popov K, Fansen K. Micromilling strategies : optimization issues. *Proc Instn Mech Engrs Part B J Eng Manuf.* 2004;218(7):731–736.

7. Henann DL, Srivastava V, Taylor HK, Hale MR, Hardt DE, Anand L. Metallic glasses: viable tool materials for the production of surface microstructures in amorphous polymers by micro-hot-embossing. *J Micromechanics Microengineering.* 2009;19(11):115030.

8. Schroers J. The Superplastic Forming of Bulk Metallic Glasses. *J Miner Met Mater Soc.* 2005;57(5):35–39.

9. Waniuk T, Schroers J, Johnson WL. Timescales of crystallization and viscous flow of the bulk glass-forming Zr-Ti-Ni-Cu-Be alloys. *Phys Rev B .* 2003;67(18):184203–184209.

10. Mani MR, Surace R, Ferreira P, Segal J, Fassi I, Ratchev S. Process Parameter Effects on Dimensional Accuracy of Micro-Injection Moulded Part. *J Micro Nano-Manufacturing Nano-Manufacturing.* 2013;1(3):031003.

11. Huang CK. Polymeric nanofeatures of 100 nm using injection moulding for replication. *J Micromechanics Microengineering.* 2007;17(8):1518–1526.

12. Monkkonen K, Hietala J, Paakkonen P, Paakkonen EJ, Kaikuranta T, Pakkanen TT, et al. Replication of Sub-Micron Features Using Amorphous Thermoplastics. *Polym Eng Sci.* 2002;42(7):1600–1608.

13. Sha B, Dimov S, Griffiths C, Packianather MS. Micro-injection moulding: Factors affecting the achievable aspect ratios. *Int J Adv Manuf Technol [Internet].* 2006;33(1-2):147–156.

14. Tosello G, Gava A, Hansen HN, Lucchetta G. Study of process parameters effect on the filling phase of micro-injection moulding using weld lines as flow markers. *Int J Adv Manuf Technol.* 2010;47(1-4):81–97.

15. Scholz SG, Griffiths CA, Dimov SS, Brousseau EB, Lalev G, Petkov P. Manufacturing routes for replicating micro and nano surface structures with bio-mimetic applications. *CIRP J Manuf Sci Technol.* 2011;4(4):347–356.

16. Tosello G, Fillon B, Azcarate S, Schoth A, Mattsson L, Griffiths C, et al. Application of different process chains for polymer microfluidics fabrication including hybrid tooling technologies , standardization and replication : a benchmark investigation within 4M Polymer Division. In: 4M 2007 Third International Conference on Multi-Material Manufacture Proceedings. 2007. p. 3–6.

17. Chen C, Chen S, Liao W, Chien R, Lin S. Micro injection molding of a micro- fluidic platform. *Int Commun Heat Mass Transf.* 2010;37(9):1290–1294.

18. Tosello G. Precision Moulding of Polymer Micro Components - Optimistation, Simulation , Tooling, Quality Control and Multi-material Application. 2008;

19. Vella PC, Dimov SS, Brousseau EB, Whiteside BR. A New Process Chain for Producing Bulk Metallic Glass Replication Masters with Micro- and Nano-scale Features. *Int J Adv Manuf Technol.* 2014;76(1-4).

20. ISO4288. Geometrical Product Specifications (GPS) -- Surface texture: Profile method -- Rules and procedures for the assessment of surface texture. 1997;

21. Leach RK. Measurement Good Practice Guide No. 37 -- The Measurement of Surface Texture using Stylus Instruments. 2001;84.

22. Joint Committee for Guides in Metrology (JCGM). Evaluation of measurement data — Guide to the expression of uncertainty in measurement (GUM). 2008.

23. Kirkup L, Frenkel B. An Introduction to Uncertainty in Measurement. 1st edn. Cambridge University Press; 2006.

24. United Kingdom Accreditation Service (UKAS). The Expression of Uncertainty and Confidence in Measurement. 2007.

25. Marinello F, Bariani P, Carmignato S, Savio E. Geometrical modelling of scanning probe microscopes and characterization of errors. *Meas Sci Technol.* 2009; 20(8):084013.

26. Tosello G, Gava A, Hansen HN, Lucchetta G, Marinello F. Characterization and analysis of weld lines on micro-injection moulded parts using atomic force microscopy (AFM). *Wear.* 2009;266(5-6):534–538.

27. Tosello G, Hansen HN, Marinello F, Gasparin S. Replication and dimensional quality control of industrial nanoscale surfaces using calibrated AFM measurements and SEM image processing. *CIRP Ann - Manuf Technol.* 2010;59(1):563–568.

28. Tosello G, Chiffre L De. Standard Traceability and Measurement Uncertainty. 2004.

29. Tosello G, Hansen HN, Gasparin S. Applications of dimensional micro metrology to the product and process quality control in manufacturing of precision polymer micro components. *CIRP Ann - Manuf Technol.* 2009;58(1):467–472.

30. Tosello G, Marinello F, Hansen HN. Characterisation and analysis of microchannels and submicrometre surface roughness of injection moulded microfluidic systems using optical metrology. *Plast Rubber Compos.* 2012;41(1):29–39.

31. Velkova V. Focused Ion Beam Technology: Implementation in Manufacturing Platforms and Process Optimisation. *Manuf. Eng. Centre, Sch. Eng.* 2011;

32. Koc M, Ozel T. Fundamentals of Micromanufacturing. In: Koc M, Ozel T, editors. Micro-Manufacturing -- Design and Manufacturing of Micro-Products. John Wiley & Sons Inc.; 2011. p. 1–23.

33. Kumar G, Staffier PA, Blawzdziewicz J, Schwarz UD, Schroers J. Atomically smooth surfaces through thermoplastic forming of metallic glass. *Appl Phys Lett .* 2010 ;97(10):101907.

34. Bardt JA, Sawyer WG. Micromolding three-dimensional amorphous metal structures. *J Mater Res.* 2007;22(2):339–343.

35. Li W, Minev R, Dimov S, Lalev G. Patterning of Amorphous and Polycrystalline Ni78B14Si8 with a Focused Ion Beam. *Appl Surf Sci.* 2007;253(12):5404–5410.

36. Beaumont JP, Nagel R, Sherman R. Sucessful Injection Moulding -- Process, Design, and simulation. 1st edn. Hanser; 2002.

37. Osswald TA, Turng LS, Gramann P. Injection Molding Handbook. 2nd edn. Hanser; 2008.

38. Giboz J, Copponnex T, Mele P. Microinjection Moulding of Thermoplastic Polymers - A review. *J Micromechanics Microengineering.* 2007;17(6):R96 – R109.

39. Attia UM, Marson S, Alcock JR. Micro-injection moulding of polymer microfluidic devices. *Microfluid Nanofluidics.* 2009;7(1):1–28.

40. Griffiths CA, Dimov SS, Scholz S, Tosello G. Cavity Air Flow Behavior During Filling in Microinjection Molding. *J Manuf Sci Eng .* 2011;133(1):011006.

41. Kumar S, Kruth JP, Van Humbeeck J, Voet A. A study of degradation of laser-sintered moulds using wear tests. *Rapid Prototyp J.* 2009 ;15(2):104–110.

42. Bergstrom J, Thuvander F, Devos P, Boher C. Wear of die materials in full scale plastic injection moulding of glass fibre reinforced polycarbonate. *Wear .* 2001;251(1-12):1511–1521.

43. Eckert J, Das J. Mechanical properties of bulk metallic glasses and composites. *J Mater Res.* 2007;22(2):285–301.

44. Gloriant T. Microhardness and abrasive wear resistance of metallic glasses and nanostructured composite materials. *J Non Cryst Solids .* 2003;316(1):96–103.

45. Huang Y, Chiu YL, Shen J, Sun Y, Chen JJJ. Mechanical performance of metallic glasses during nanoscratch tests. *Intermetallics.* 2010;18(5):1056–1061.

46. Liang S, He JY, Chu WY, Li JX, Sun DB, Qiao LJ. Nanowear of a Zr-based Bulk Metallic Glass/ Nanocrystalline Alloy. *Trans Mater Heat Treat.* 2004;25(5):1195 – 1199.

47. Wang JG, Choi BW, Nieh TG. Nano-scratch Behavior of a Zr-10Al-5Ti-17.9Cu-14.6Ni amorphous alloy. *J Mater Res.* 2000;15(4):913–922.

48. Greer AL, Rutherford KL, Hutchings IM. Wear resistance of amorphous alloys and related materials. *Int Mater Rev.* 2002 ;47(2):87–112.

49. Löffler JF. Bulk metallic glasses. *Intermetallics .* 2003;11(6):529–540.

50. Suryanarayana C, Inoue A. Bulk Metallic Glasses. 1st edn. CRC Press Taylor & Francis Group; 2011.

51. Hess PA, Dauskardt RH. Mechanisms of elevated temperature fatigue crack growth in Zr–Ti–Cu–Ni–Be bulk metallic glass. *Acta Mater.* 2004;52(12):3525–3533.

52. Wang GY, Liaw PK. Effects of partial crystallization on compression and fatigue behavior of Zr-based bulk metallic glasses. *J Mater Res.* 2007;22(2):493–500.

53. Wang GY, Liaw PK, Yokoyama Y, Inoue a., Liu CT. Fatigue behavior of Zr-based bulk-metallic glasses. *Mater Sci Eng A.* 2008;494(1-2):314–323.

54. Wang G, Liaw PK, Yokoyama Y, Freels M, Inoue A. Investigations of the Factors that Affected Fatigue Behavior of Zr-Based Bulk-Metallic Glasses. *Adv Eng Mater .* 2008;10(11):1030–1033.

55. Wang GY, Liaw PK, Yokoyama Y, Inoue A. Size effects on the fatigue behavior of bulk metallic glasses. *J Appl Phys .* 2011;110(11):113507.

56. Wang GY, Liaw PK. Fatigue and Fracture Behavior. In: Miller M, Liaw P, editors. Bulk Metallic Glasses. Springer; 2010. p. 169–203.

57. Clark W, Horrell K, Rogelstad T, Spagon P. SEMATECH Qualification Plan Guidelines for Engineering. 1995;94.

58. Montgomery DC. Design and Analysis of Experiments. 7th edn. John Wiley & Sons Inc.; 2009.

59. Telford JK. A Brief Introduction to Design of Experiments. *John Hopkins APL Tech Dig.* 2007;27(3):224–232.

60. Kumar G, Schroers J. Write and erase mechanisms for bulk metallic glass. *Appl Phys Lett.* 2008;92(3):31901–31903.

61. Packard CE, Schroers J, Schuh CA. In situ measurements of surface tension-driven shape recovery in a metallic glass. *Scr Mater.* 2009;60(12):1145–1148.

62. Hansen HN, Hocken RJ, Tosello G. Replication of micro and nano surface geometries. *CIRP Ann - Manuf Technol.* 2011;60(2):695–714.

63. Leyland A, Matthews A. On the significance of the H/E ratio in wear control: a nanocomposite coating approach to optimised tribological behaviour. *Wear .* 2000;246(1-2):1–11.